DRAFT FOR OMAE 2024, SINGAPORE

DRAFT: THE SPAR MODEL: A NEW PARADIGM FOR MULTIVARIATE EXTREMES. APPLICATION TO JOINT DISTRIBUTIONS OF METOCEAN VARIABLES

E.B.L. Mackay,
University of Exeter, UK

C.J.R. Murphy-Barltrop,
Technische Universität Dresden, Germany
ScaDS.AI, Germany

P. Jonathan,
Lancaster University, UK
Shell Research Limited, UK

ABSTRACT

This paper presents the application of a new multivariate extreme value model for the estimation of metocean variables. The model requires fewer assumptions about the forms of the margins and dependence structure compared to existing approaches, and provides a flexible and rigorous framework for modelling multivariate extremes. The method involves a transformation of variables to polar coordinates. The tail of the radial variable is then modelled using the generalised Pareto distribution, with parameters conditional on angle, providing a natural extension of univariate theory to multivariate problems. The resulting model is referred to as the semi-parametric angular-radial (SPAR) model. We consider the estimation of the joint distributions of (1) wave height and wave period, and (2) wave height and wind speed. We show that the SPAR model provides a good fit to the observations in terms of both the marginal distributions and dependence structures. The use of the SPAR model for estimating long-term extreme responses of offshore structures is discussed, using some simple response functions for floating structures and an offshore wind turbine with monopile foundation. We show that the SPAR model is able to accurately reproduce response distributions, and provides a realistic quantification of uncertainty.

1 INTRODUCTION

Many design problems in offshore engineering require estimates of the joint extremes of metocean variables, such as winds, waves, currents and water levels. Joint extremes of metocean variables are often quantified in terms of environmental contours [1]. Some types of environmental contours can be estimated without knowing the joint density of the variables [2, 3]. However, in other applications, such as full long-term extreme response analysis (e.g. [4]), a model is needed for the joint density. Estimating the joint density in extreme regions of the variable space is subject to large uncertainties [5, 6]. A wide range of methods have been proposed for estimating the joint density function of metocean variables; a relatively recent review is presented in [7]. At present, the most commonly-used approaches are global hierarchical models and copula models. These models can be applied in any number of dimensions, but for simplicity we shall restrict the discussion to two-dimensional cases. In the global hierarchical model, the joint density function $f_{X,Y}$ of variables X, Y is written in conditional form as

$$f_{X,Y}(x,y) = f_X(x) f_{Y|X}(y|x), \tag{1}$$

where $f_X(x)$ is the marginal density of X and $f_{Y|X}(y|x)$ is the density of Y conditional on $X = x$. Usually, a parametric form is assumed for both f_X and $f_{Y|X}$, with popular choices being Weibull and log-normal models [8, 9]. The parameters of the conditional distribution are then modelled as a function of x. There are several drawbacks to this approach. For example, assuming a model for the bulk of the observations does not guarantee a good fit to the tail of the distribution, which is the region of interest when estimating extreme responses. Moreover, the model for the conditional dependence structure is not based on any physical or mathematical principles, and hence provides no rationale for extrapolating outside the range of observations. These limitations mean that fitted models obtained from this approach are often in poor agreement with observations [6].

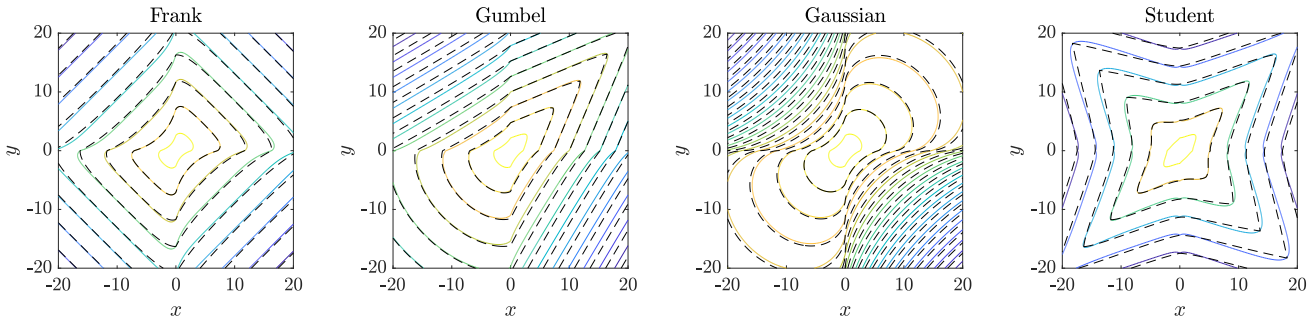

FIGURE 1. CONTOUR PLOTS OF JOINT DENSITIES OF VARIOUS COPULAS ON LAPLACE MARGINS. ALL COPULAS HAVE PEARSON CORRELATION COEFFICIENT $\rho = 0.6$. STUDENT-T COPULA HAS $\nu = 2$ DEGREES OF FREEDOM. SOLID LINES: TRUE ISODENSITY CONTOURS AT LOGARITHMIC INCREMENTS. DASHED LINES: ISODENSITY CONTOURS OF SPAR APPROXIMATIONS AT THE SAME DENSITY VALUES.

In copula-based approaches, the joint density function is expressed as $f_{X,Y}(x,y) = f_X(x)\, f_Y(y)\, c(F_X(x), F_Y(y))$, where f_X, f_Y, F_X, F_Y are the marginal density and distribution functions, and c is the copula density function (e.g. [10, 11]). As well as assuming a form for the margins, a parametric form for the copula is also assumed. Common choices for the copula include Frank, Gumbel, Gaussian and Student-t [12–14]. Examples of the joint density functions for these four copulas are shown in Figure 1, with standard Laplace margins, i.e. $f_X(z) = f_Y(z) = \frac{1}{2}\exp(-|z|)$, $z \in \mathbb{R}$. In each case, the copula parameters have been selected so that the Pearson correlation coefficient is $\rho = 0.6$. It is evident that different choices of copula can lead to large differences in joint tail behaviour. Moreover, usually there is no a-priori reason to suppose that the dependence structure in observations follows a particular parametric form.

Various methods based on multivariate extreme value theory have been proposed; see [15, 16] for an overview of the applications in an oceanographic context. Possibly the most popular choice for metocean variables is the conditional extremes model [17], which can be used to estimate the joint distribution of variables conditional on at least one variable being large. Example metocean applications include [18, 19]. The key limitation of this approach is that it only characterises the region of variable space where the conditioning variable is large, and inferences made using different conditioning variables are not necessarily consistent [20]. A further limitation of this method (and other methods in the multivariate extremes literature), is that it requires a transformation of the margins to a standard scale. This requires first estimating the marginal distributions for each variable – a process which is subject to uncertainty.

In this paper, we discuss the application of a new method, which overcomes the limitations of existing approaches and provides a general framework for modelling multivariate extremes. The model is referred to as the Semi-Parametric Angular-Radial (SPAR) model. The SPAR model provides a framework for estimating multivariate extremes that does not require any assumptions about the form of the margins or dependence structure, and provides a rational means for extrapolating outside the range of observations. Moreover, the model is only fitted to extreme observations, meaning that no assumptions are required about the bulk of the distribution. The SPAR model can either be applied on transformed margins, or on the original marginal scale, removing the need to fit marginal models. Theoretical aspects of the SPAR model have been presented recently in [21], and a detailed discussion of SPAR model inference is presented in [22]. The purpose of this paper is to provide a more engineering-focused description of the SPAR model, and demonstrate its application for estimating joint extremes of metocean variables and extreme responses of offshore structures.

The paper is organised as follows. A brief overview of the theory is presented in Section 2, and inference is discussed in Section 3. In Section 4, we discuss the application of the SPAR model to the estimation of the joint extremes of (1) wave height and wave period, and (2) wave height and wind speed. In Section 5, we consider the long-term extreme response distribution for some simple response functions, using the fitted SPAR models. We conclude with a discussion in Section 6.

2 THEORY

2.1 Model definition

The SPAR model is an extension of the univariate peaks-over-threshold (POT) method to the multivariate setting. The method involves a transformation of the variables to polar coordinates. In the present work, we will restrict our attention to standard polar coordinates in two dimensions, but more general polar coordinate systems can also be used (see [21] for a discussion). Define radial and angular variables as $R = (X^2 + Y^2)^{1/2}$, $\Theta = \text{atan2}(X,Y)$, where atan2 is the four-quadrant inverse tangent function. Suppose that random vector (X,Y) has continuous joint density function $f_{X,Y}$, with simply connected support, containing the point $(0,0)$. Then the joint density of (R,Θ) is given

by

$$f_{R,\Theta}(r,\theta) = r \cdot f_{X,Y}(r\cos(\theta), r\sin(\theta)). \quad (2)$$

In a similar manner to global hierarchical models (1), the angular-radial joint density can be written in conditional form:

$$f_{R,\Theta}(r,\theta) = f_{\Theta}(\theta) f_{R|\Theta}(r|\theta) \quad (3)$$

In this form, the problem of modelling multivariate extremes is transformed to that of modelling an angular density $f_{\Theta}(\theta)$ and the tail of the conditional radial density $f_{R|\Theta}(r|\theta)$. For a given angle θ, the density $f_{R|\Theta}(r|\theta)$ is univariate. Univariate extreme value theory suggests that a suitable model for the tail of $f_{R|\Theta}(r|\theta)$ is the generalised Pareto (GP) distribution, with parameters conditional on angle (e.g. [23]). This motivates the SPAR model, first introduced in [24], whereby parametric and non-parametric models are used to model the conditional radial and angular distributions, respectively. Define a threshold function $u(\theta) > 0$ to be the quantile of $R|(\Theta = \theta)$ at exceedance probability $\zeta \in (0,1)$ (where ζ is close to 0), i.e. the solution of $\zeta = \Pr(R > u(\theta)|\Theta = \theta)$. Then the SPAR model can be written

$$f_{R,\Theta}(r,\theta) = \zeta f_{\Theta}(\theta) f_{GP}(r;\xi(\theta),\sigma(\theta),u(\theta)), \quad r > u(\theta), \quad (4)$$

where f_{GP} is the GP density function, and $\xi(\theta) \in \mathbb{R}$ and $\sigma(\theta) > 0$, are the shape and scale parameters, given as functions of the angle θ. The GP density function is given by

$$f_{GP}(r;\xi,\sigma,u) = \begin{cases} \frac{1}{\sigma}\left(1+\xi\frac{r-u}{\sigma}\right)^{-1-\frac{1}{\xi}}, & \xi \neq 0 \\ \frac{1}{\sigma}\exp\left(\frac{r-u}{\sigma}\right), & \xi = 0. \end{cases} \quad (5)$$

The support is $0 \leq r \leq r_F$, where the upper end point is $r_F = \infty$ for $\xi \geq 0$ and $r_F = u - \sigma/\xi$ for $\xi < 0$.

For the purposes of inference, it is also assumed that both the angular density f_{Θ} and GP parameter functions $\xi(\theta)$, $\sigma(\theta)$ and $u(\theta)$ are finite and continuous with angle. It was shown in [21] that these assumptions are valid for a wide range of copulas on Laplace margins. For parametric copulas, the asymptotic values of the GP parameter functions can be derived and used to compare the SPAR model for the density to the true values. This is shown in Figure 1 for the cases of the Frank, Gumbel, Gaussian and Student-t copulas on Laplace margins (see [21] for details). The SPAR representation is in good agreement with the theoretical values, showing that the model can represent a wide range of dependence structures, without having to make prior assumptions about a particular parametric forms of the copula. Furthermore, the SPAR approach has the advantage over the conditional extremes method in that it can characterise all extreme regions of the variable space in a single inference. It can also be shown that various other methods for estimating multivariate extremes, such as [25–27] are special cases of the SPAR model, and that SPAR provides a more flexible framework than existing techniques [21].

2.2 Use of the model

Once the angular density and GP parameter functions have been estimated, equations (2) and (4) can be combined to obtain the SPAR estimate of the joint density in the original variable space for observations satisfying $r > u(\theta)$:

$$f_{X,Y}(r\cos(\theta), r\sin(\theta)) = \frac{\zeta}{r} f_{\Theta}(\theta) f_{GP}(r;\xi(\theta),\sigma(\theta),u(\theta)). \quad (6)$$

The SPAR model also provides an explicit means for calculating a contour which has exceedance probability $\beta \leq \zeta$. The radius of this contour at angle θ is simply the quantile of the GP distribution at exceedance probability β/ζ, given by

$$r_{\beta}(\theta) = u(\theta) + \frac{\sigma(\theta)}{\xi(\theta)}\left((\beta/\zeta)^{-\xi(\theta)} - 1\right) \quad (7)$$

This contour is defined in terms of the probability of an observation falling anywhere outside the region, or the 'total exceedance probability'. As such, these contours are more conservative than those defined in terms of marginal exceedance probabilities, such as IFORM contours (or variants thereof) [28].

Calculating marginal and joint probabilities from the SPAR model involves integrating the joint density over various angular and radial ranges. However, probabilities can be estimated empirically by simulating from the estimated model. Simulation under the SPAR model is straightforward. We start by generating a random number p, uniformly-distributed in $[0,1]$. A random angle $\theta \in [0, 2\pi)$ can then be calculated by applying the probability integral transform so that $\theta = F_{\Theta}^{-1}(p)$. A corresponding radial value r, is then simulated as a random value from the GP distribution with parameter vector $(\xi(\theta),\sigma(\theta),\mu(\theta))$. The pair (θ, r) is then a random sample from the SPAR model. This can be converted back to the original variable space using the inverse transformation $(x,y) = (r\cos(\theta), r\sin(\theta))$.

3 INFERENCE

Inference for the SPAR model can be viewed as a non-stationary POT analysis, for which there are many examples in

the literature [29–33]. The parameter functions of the GP model for the tail of the conditional radial density are estimated using the EVGAM package [31]. This approach uses generalised additive models (GAMs) to represent the variation of the GP threshold, scale and shape parameters as functions of angle. GAMs are a flexible class of regression models that allow for complex, non-linear relationships between response and predictor variables [34]. Full details of this inference method are given in [22] and a GitHub repository of the associated code is available at https://github.com/callumbarltrop/SPAR. In this section we provide high-level details only. We start by discussing inference for the angular density in Section 3.1, then discuss inference for the conditional radial density in Section 3.2. The selection of tuning parameters for the model is discussed in Section 3.3.

3.1 Angular density

As the angular density is assumed to be finite and continuous, it is readily amenable to non-parametric estimation methods. In the present work, we use kernel density (KD) estimation. Given a sample $\{\theta_1,...,\theta_n\}$, the KD estimate of the angular density at angle $\theta \in [0,2\pi)$ is

$$\hat{f}_\Theta(\theta) = \frac{1}{n}\sum_{i=1}^{n} K_h(\theta,\theta_i), \tag{8}$$

where K_h denotes some kernel defined on a circular domain, with bandwidth parameter h. The bandwidth controls the smoothness of the estimate with smoothness increasing with bandwidth. For the examples considered in Section 4, we have used a von Mises kernel, given by

$$K_h(\theta,\theta_i) = \frac{1}{2\pi I_0(1/h)} \exp\left(\frac{\cos(\theta-\theta_i)}{h}\right),$$

where I_0 is the modified Bessel function of the first kind of order zero. As $h \to 0$, the von Mises kernel converges to a Gaussian kernel with variance h. This choice of kernel was shown to work well for the theoretical examples considered in [22].

We note that the angular density could also be estimated using GAMs, using a similar approach to that in [29, 30]. Whilst this is more elegant in that the same approach is used to model both the angular and radial components, we have opted to use a KD model in the present work due to its simplicity.

3.2 Conditional radial density

In the GAM framework, an arbitrary function $g(\theta)$ (which could represent the threshold, scale or shape parameter) is represented as a sum of smooth basis functions specified at a finite number of locations, known as knots:

$$g(\theta) = \sum_{j=1}^{k} \beta_j B_j(\theta), \quad \theta \in [0,2\pi), \tag{9}$$

where $B_j(\theta)$ are the basis functions, $\beta_j = g(\phi_j)$ is the value of the function at knot location $\phi_j \in [0,2\pi)$, and $k \in \mathbb{N}$ is the number of knots (also referred to as the basis dimension). A wide variety of smooth basis functions exist [35]. In the present application we have used cyclic cubic regression splines, which ensure that the GP parameter function estimates are periodic with angle. In practice, the values of β_j are not known, and are estimated as part of the inference. EVGAM uses a penalised maximum likelihood method to estimate the coefficients β_j for the GP parameter functions. The penalty terms are defined in terms of the roughness of the solution, thus avoiding over-fitting. The optimal choice of roughness penalties are estimated using a cross-validation procedure. As with univariate POT analysis, the threshold is selected prior to fitting the GP distribution. In the multivariate case, threshold function is estimated using quantile regression [36, 37], with a GAM representation for the model parameters.

The GP parameter functions estimated from EVGAM can be compared to estimates from a local stationary inference to check their plausibility. The local stationary inference is conducted for a grid of angular values. At each angle, a stationary GP model is fitted to the m nearest observations (in terms of angle). The assumption that the local distribution is stationary is an approximation. The choice of m is a bias-variance trade-off: smaller values lead to higher estimation variance, while larger values make the assumption of stationarity less valid. In practice, the local stationary inference is only used for verification of the GAM estimates.

3.3 Selection of tuning parameters

Application of the SPAR model requires the selection of the following tuning parameters:

1. kernel bandwidth, h, for the angular density;
2. threshold exceedance probability, ζ;
3. spline basis dimension, k, and knot locations $\phi_1,...,\phi_k$.

In principle, optimal values of all of these tuning parameters could be estimated from the data. However, to simplify the inference, we have opted to select these manually in the present implementation. For the kernel bandwidth, as with any application of kernel density estimation, the goal is to select h as small as possible, while avoiding over-fitting. In the examples presented in Section 4, it was found that a bandwidth of $h = 0.02$ was sufficient to represent the observed angular densities. The choice of threshold exceedance probability is directly analogous to the case in univariate analyses. That is, the threshold must be high enough

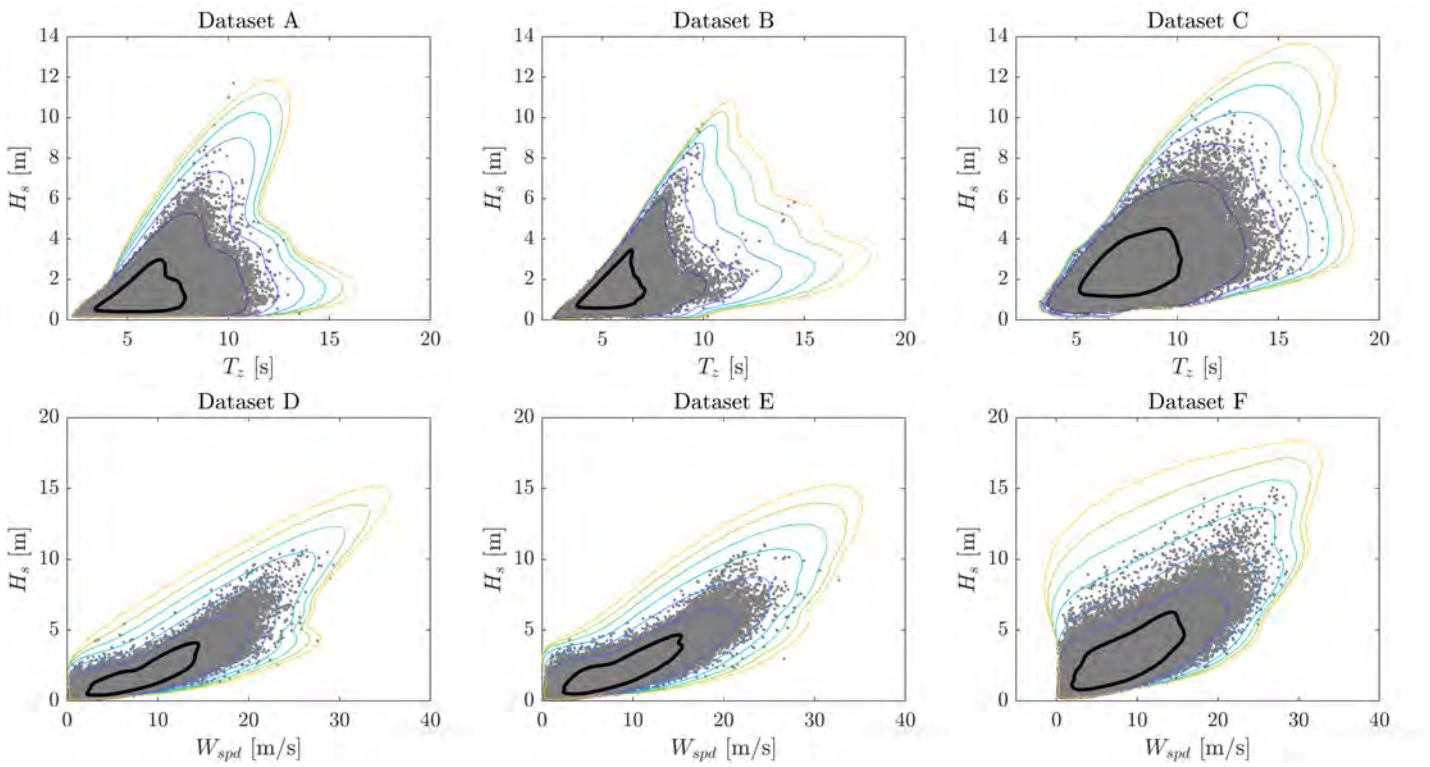

FIGURE 2. COMPARISON OF OBSERVATIONS (DOTS) AND ISODENSITY CONTOURS FROM FITTED SPAR MODELS (COLOURED LINES). THRESHOLDS ARE SHOWN IN THICK BLACK LINE. ISODENSITY CONTOURS ARE AT EQUAL LOGARITHMIC INCREMENTS: $10^{-3}, 10^{-4}, ..., 10^{-8}$.

such that the GP model is a reasonable approximation. Using too low a threshold will risk the model being misspecified, whilst too high a threshold will reduce the number of exceedances, increasing variance in the parameter estimates. A wide range of methods have been proposed for threshold selection; see [38] for a review and [39] for more recent developments. In the present work, the SPAR model was fitted for various threshold choices and diagnostic plots (discussed below) were checked to assess goodness of fit. For the examples considered here, we found that a threshold exceedance probability of $\zeta = 0.3$ was reasonable.

Selecting an appropriate basis dimension is essential for ensuring accuracy and flexibility in spline modelling procedures. Selecting too few knots may result in functional estimates that do not capture the underlying covariate relationships. Provided the basis dimension is sufficiently large, the resulting functional estimates should be relatively insensitive to the exact value. This is due to the roughness penalties, which prevent over-fitting, thus dampening the effect of adding additional basis knots to the spline formulations [34]. For the examples considered here, we found that using $k = 35$ knots was sufficient for the threshold and scale functions, and $k = 12$ knots was used for the shape parameter functions. The knot locations have been defined at equally spaced empirical quantiles of Θ. This ensures that the knot spacing is closer in regions where more data has been observed. Moreover, assuming the basis dimension is large enough, model fit should be relatively insensitive to the precise location of knots [34]. We note that other spline representations and inference techniques allow the estimation of the optimal number of spline knots and their locations (e.g. [32]), although this is not considered further here.

4 JOINT EXTREMES OF METOCEAN VARIABLES

In this section we demonstrate the application of the SPAR model to the datasets provided as part of the recent benchmarking exercise for environmental contours [5]. This comprises three datasets of wave buoy measurements of significant wave height (H_s) and zero-crossing period (T_z) from wave buoys around the US coastline, and three datasets of wind speed (W_{spd}) and significant wave height for locations in the North Sea from the coastDat-2 hindcast [40]. All datasets have 1-hour timesteps and observations will therefore be serially correlated. The effect of this is discussed further below. Dataset C from [5] was from a buoy in the Gulf of Mexico, an area affected by hurricanes. These types of datasets typically require careful treatment for hurricane-generated waves (see e.g. [41]). Therefore, for the present study we have replaced Dataset C with another wave

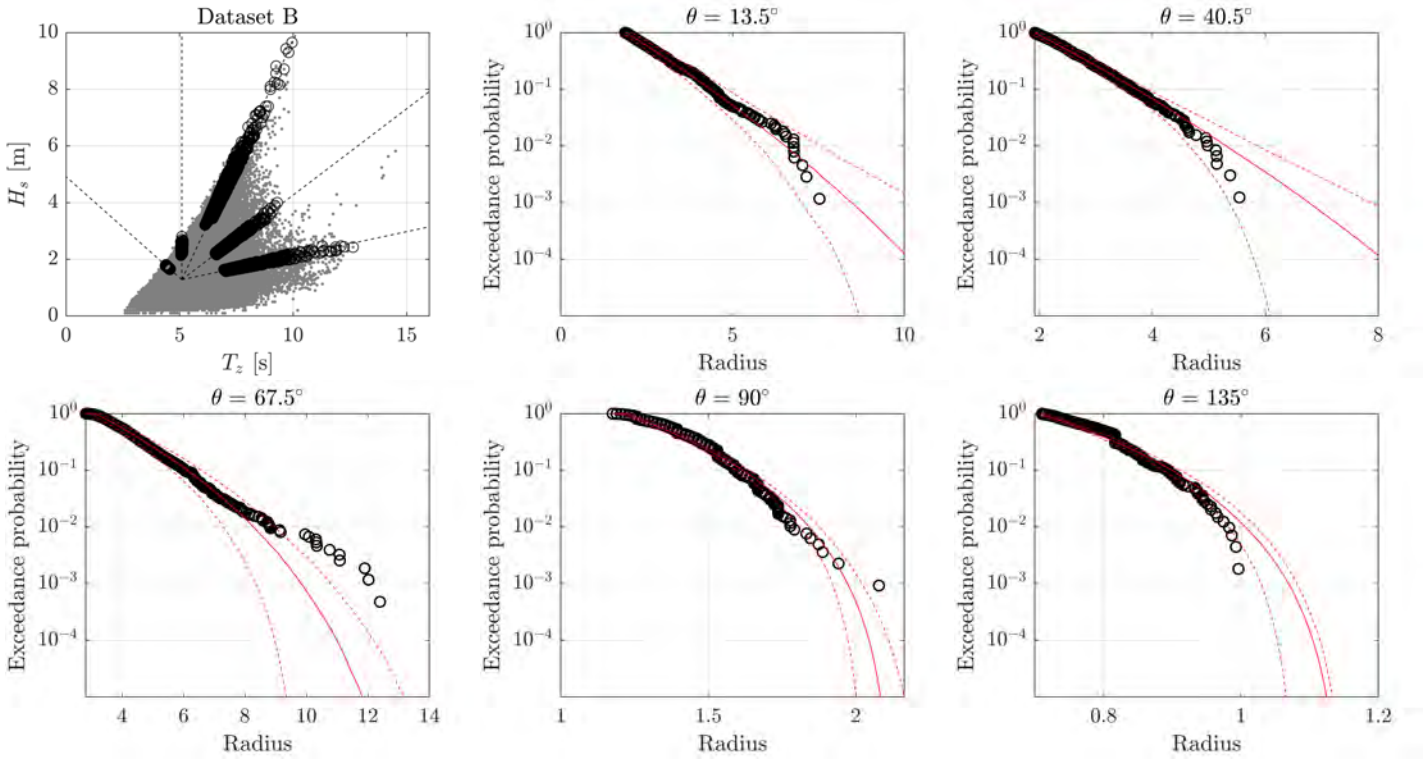

FIGURE 3. COMPARISON OF CONDITIONAL RADIAL EXCEEDANCE PROBABILITIES AT VARIOUS ANGLES, FROM OBSERVATIONS (CIRCLES) AND SPAR MODELS (RED LINES) FOR DATASET B. DASHED LINES INDICATE 95% BOUNDS FOR MODEL QUANTILES. TOP LEFT PLOT SHOWS ALL OBSERVATIONS (DOTS) AND THRESHOLD EXCEEDANCES USED AT EACH ANGLE (CIRCLES).

Dataset	Source	Variables	Start	End
A	NDBC buoy 44007	H_s, T_z	16/02/1982	31/12/2022
B	NDBC buoy 44024	H_s, T_z	29/04/1991	31/12/2022
C	NDBC buoy 46014	H_s, T_z	01/04/1981	31/03/2023
D, E, F	coastDat-2 hindcast	H_s, W_{spd}	01/01/1965	31/12/1989

TABLE 1. DESCRIPTION OF METOCEAN DATASETS.

buoy record from the US West coast, NDBC buoy number 46014. Details of the datasets are given in Table 1. As different variables can have very different scales, we begin by centering and scaling the variables. For random variables X and Y, define normalised variables $(\tilde{X},\tilde{Y}) = ((X-m_X)/s_X,(Y-m_Y)/s_Y)$, where m_X, m_Y, s_X and s_Y are the sample mean and standard deviation of X and Y respectively. We define our polar coordinates in terms of the normalised variables, thus ensuring that the origin is within the body of the data. As this is a rescaling of the data, rather than a marginal transformation, it is subject to lower uncertainties, and makes no assumptions about the distribution of the data.

For each dataset, the SPAR model was fitted using the inference procedure described in Section 3. To quantify the uncertainty, the datasets were resampled 200 times, and the SPAR model was fitted to each resampled dataset. As the hourly-observations are serially correlated, a block bootstrap [42] was used, with a block length of 4 days. Here we consider various diagnostic plots to assess the quality of the fitted models. Comparisons of the observations with isodensity contours from the fitted SPAR models are shown in Figure 2. In general, the isodensity contours provide a good description of the location of the observations. Although no information about physical constraints has been used to inform the model fitting, the models are able to capture various features of the data. Firstly, the lower bounds on all variables is zero – this is captured in datasets A-E, but the model for dataset F does predict slightly negative wind speeds at higher values of H_s. This could potentially be prescribed as a hard constraint in the model. However, given that this part of the distribution is of less interest, and any negative data can easily be removed from estimates, we have not attempted to apply this constraint in the present work. Secondly, the SPAR models for the wave height-period data capture the limiting effect of the wave steepness, defined as $s = 2\pi H_s/(gT_z^2)$, where g is acceleration due to gravity. When the steepness exceeds a certain value, waves break, limiting the wave height at a given period. The

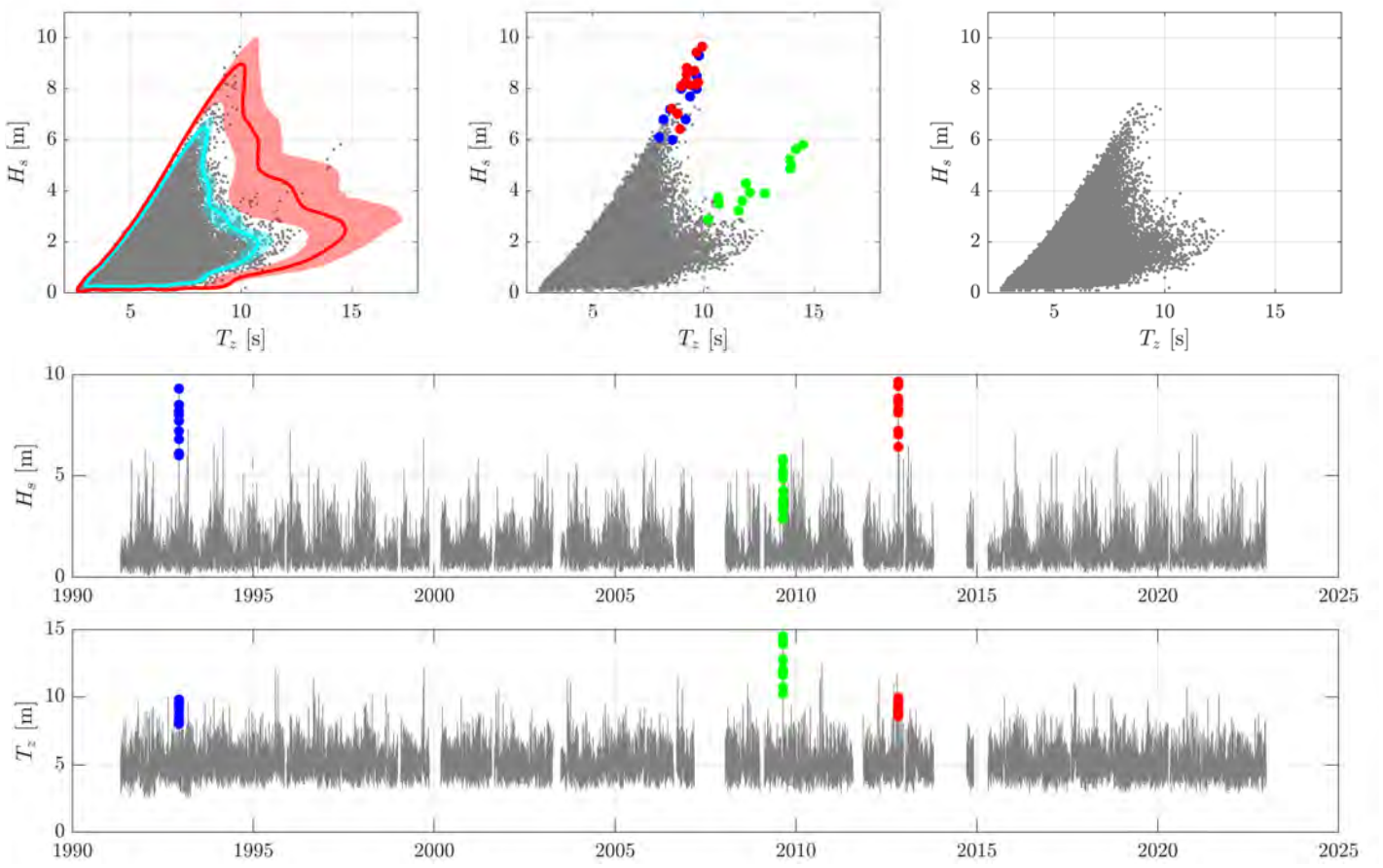

FIGURE 4. ANALYSIS OF UNCERTAINTIES IN SPAR CONTOURS FOR DATASET B. TOP LEFT: CONTOURS (SOLID LINES) AND 95% BOUNDS FOR EXCEEDANCE LEVELS OF 10^{-2} AND 10^{-4}. TOP MIDDLE: OBSERVATIONS WITH THREE 12-HOUR EVENTS HIGHLIGHTED (COLOURED POINTS). TOP RIGHT: OBSERVATIONS WITH THREE 12-HOUR EVENTS EXCLUDED. LOWER PLOTS: TIME SERIES OF H_s AND T_z WITH THREE 12-HOUR EVENTS HIGHLIGHTED, EMPHASISING THE SERIAL CORRELATION AND THE NEED TO ACCOUNT FOR THIS WHEN ESTIMATING UNCERTAINTIES.

limiting value of s is dependent on wind speed and water depth (among other factors), but values exceeding $s = 0.1$ are rare. The ability of the SPAR models to capture the limiting steepness is evident in the tight grouping of isodensity contours on the upper left side of the distributions.

A more localised assessment of the quality of the fitted model can be made by comparing the tails of the observed and modelled radial distributions over small angular ranges. Figure 3 shows an example for dataset B. Five angles have been selected to illustrate various features of the data. For each angle observations are selected within a $\pm 2^\circ$ range. At 13.5° and 40.5°, the model agrees well with the observations, within the estimated uncertainty. At 90° and 135°, there is some small discrepancy between the model and observations, although the uncertainty range is much smaller, due to the limiting effects of wave steepness at these angles. At 67.5°, which corresponds to the largest wave heights, there is a larger discrepancy between the model and largest observations. Note that all observations exceeding the upper 95% bound at this angle come only from two storms. This is illustrated in Figure 4, which highlights two 12-hour periods (blue and red points), centred on these two storm peaks. Similarly, the largest observations of wave period all come from a single event (highlighted green). For comparison, the observations with these three 12-hour periods removed are shown in the upper right plot of Figure 4. As the model uncertainty is estimated using a block bootstrap, it accounts for these hourly observations coming from discrete events. The upper left plot of Figure 4 shows exceedance contours calculated using (7) at probability levels 10^{-2} and 10^{-4} together with 95% bounds. There is very low uncertainty on the high-steepness side of the contour, whilst on the upper side and right side the uncertainty range is wider, reflecting the longer tails of the conditional radial distribution in these ranges. Similar behaviour was observed for datasets A and C (not shown).

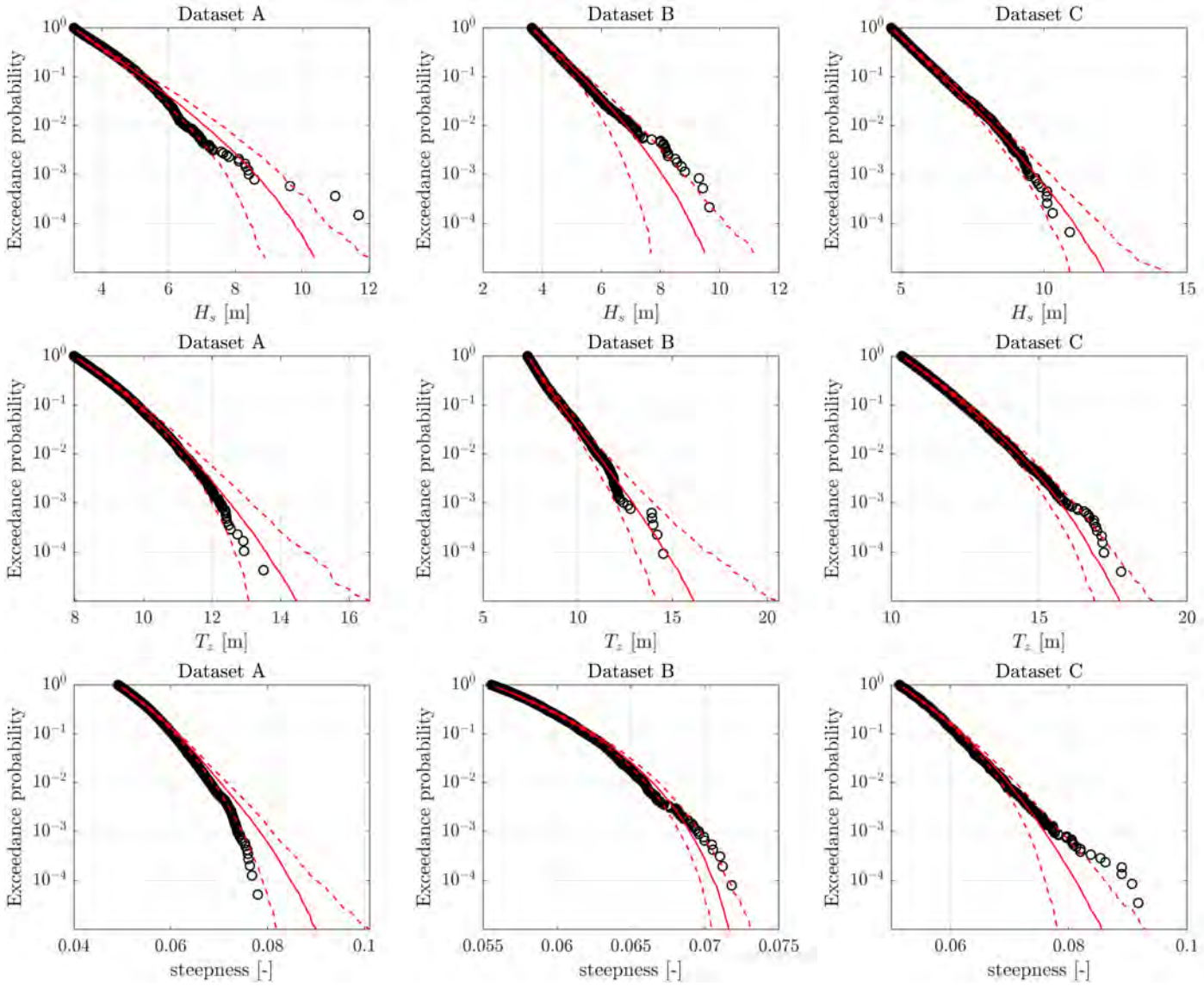

FIGURE 5. COMPARISON OF MARGINAL EXCEEDANCE PROBABILITIES FROM OBSERVATIONS (CIRCLES) AND SPAR MODELS (RED LINES) FOR WAVE HEIGHT-PERIOD DATASETS. DASHED LINES INDICATE 95% BOUNDS ON MODEL QUANTILES.

Finally, we compare the marginal exceedance probabilities from the SPAR models and observations. To ensure consistency, both observed and simulated data are restricted to exceedances of the highest value along the threshold function in the relevant dimension. That is, for the x-direction, observations are restricted to those for which $x > \max_{\theta\in(-\pi,\pi]}(u(\theta)\cdot\cos(\theta))$. Figure 5 shows exceedance probabilities from observations and fitted models for H_s, T_z and s for each dataset. Generally, the models and observations are in good agreement. We emphasise that the margins have not been estimated directly, but are outputs from the fitted SPAR models (for the tail regions). Despite not fitting the marginal tails directly, the SPAR models still perform well. As discussed above, for dataset B, all observations with $H_s > 7.5$ m come from two storms. Similarly, for dataset A, the observations with $H_s > 10$ m come from a single storm. The SPAR models are in good agreement with the observations for the largest values of T_z for all datasets. For the steepness, the model slightly over-predicts the steepness for dataset A, although the model values are still realistic. For dataset C, the model slightly under-predicts the largest values of wave steepness. However, for this dataset, the largest values of steepness occur in smaller wave heights, with $H_s < 4$ m, so

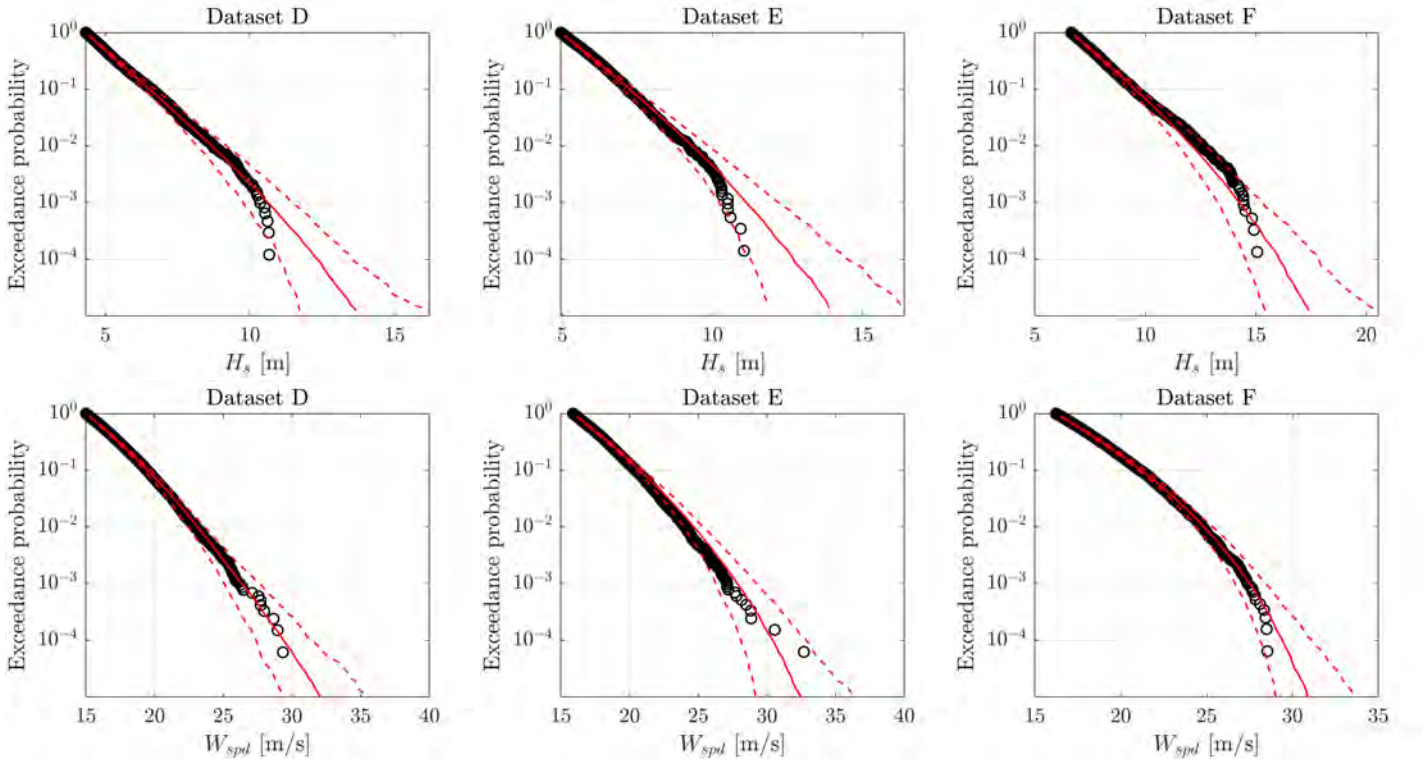

FIGURE 6. COMPARISON OF MARGINAL EXCEEDANCE PROBABILITIES FROM OBSERVATIONS (CIRCLES) AND SPAR MODELS (RED LINES) FOR WIND-WAVE DATASETS. DASHED LINES INDICATE 95% BOUNDS ON MODEL QUANTILES.

these conditions are less likely to affect structural design. Figure 6 shows marginal exceedance probabilities for datasets D-F. In these cases, the agreement is generally very good, with the fitted models agreeing with observations to within the estimated uncertainty.

5 LONG-TERM EXTREME RESPONSES

The analysis in the previous section has considered the fit of the SPAR model to observations. From an engineering perspective, it is usually the response of a structure that is of primary interest, rather than the environmental conditions themselves. To assess the SPAR method further, we consider how well the fitted model can capture response distributions for some simple response functions. In the case of the joint distributions of H_s and T_z, we consider three response functions used in [6] for the vertical bending moment (VBM) on various vessels. The normalised responses are shown in Figure 7 (a) as functions of T_z, and responses are assumed to vary linearly with H_s. The peak responses occur at approximately 5.9 s, 8.5 s and 11.8 s and are relatively broad-banded. Although the responses are for VBM on particular vessels, they can be considered as representative of a wider range of responses of offshore structures. For the joint distributions of H_s and W_{spd}, we consider the mudline overturning moment on a 5 MW offshore wind turbine using the response function derived in [43]; this is illustrated in Figure 7 (b). The response function given in [43] is also dependent on wave period, but we have removed this dependence by assuming a constant steepness of 0.03. The response function is also stochastic, so to avoid adding additional random effects to the comparison, we have used the median value for each environmental condition. There is a discontinuity in the response surface at $W_{spd} = 25$ m/s, which corresponds to the cut-out wind speed of the turbine. For winds above this speed, the turbine is shut down and the blades are feathered to reduce loading. At lower wave heights, this causes a reduction in loading. However, at very high wave heights, an increased response is observed above the cut-out speed, as the rotor is no longer damping the wave-induced motions of the tower.

Figure 8 compares exceedance probabilities for responses calculated from observations and simulations from the fitted SPAR models for datasets A-C. As the SPAR model is only fitted to threshold exceedances, the observed sample is restricted to the same range. We have also restricted both samples to values exceeding the mean H_s, to avoid including smaller responses in the comparison. For dataset C the responses from models and observations are in good agreement. For datasets A and B the

agreement is generally good, but with some discrepancies, which are broadly inline with those shown for the marginal quantities in Figure 5. Figure 9 compares exceedance probabilities for the wind turbine response function calculated from observations and models for datasets D-F. In all cases, the models agree well with observations, indicating that they provide an accurate representation of the joint distribution in the relevant areas of the variable space.

6 DISCUSSION AND CONCLUSIONS

This paper has demonstrated the application of the SPAR model for estimating the joint distribution of metocean variables. The SPAR model has several advantages over existing methods. Firstly, no assumptions are required about either the form of the margins or dependence structure, and the model can be applied on the original scale of the data, without a marginal transformation. Secondly, the model provides a rigorous basis for extrapolating outside the range of observations based on extreme value theory. And thirdly, in contrast to existing methods, the same model formulation is applicable in different applications, removing the need for ad hoc assumptions. By transforming the variable space to polar coordinates, the SPAR approach reframes multivariate extreme value modelling as a natural extension of univariate extremes, with angular dependence.

The SPAR model was shown to provide a good representation of the joint extremes of wave heights and periods, and wave heights and wind speeds, using data for several locations. Accuracy of the fitted SPAR models was also assessed using simple response functions, relevant to offshore engineering applications. In the examples considered, the response distributions calculated from the models were in good agreement with those from observations, giving confidence in the use of the models in engineering applications.

The examples considered here are for two-dimensional problems. The SPAR approach is also applicable in higher dimensions. However, extending the inference to higher dimensions becomes more computationally challenging due to the number of parameters involved. The present work has not considered including covariate effects such as seasonality or directionality. However, as inference for the SPAR model can be viewed as non-stationary POT, where radius is the response variable and angle is the covariate, periodic covariates such as season and direction can be included as additional 'angles', treated in the same way as in existing models (e.g. [44, 45]).

A limitation of the present model is that it does not provide information about serial correlation in the observations (although serial correlation is accounted for in the uncertainty calculations). This is usually accounted for by 'declustering' the data, and only modelling peak values. However, in multivariate applications, what constitutes a 'peak value', depends on which variable is of interest, since extremes of each variable do not necessarily occur simultaneously; see [3, 46] for further discussion. Modelling the distribution of other values, conditional on a peak value in a similar manner to [47], may provide a suitable solution, but this will require further investigation.

Finally, the sensitivity of the inference to the choice of origin and polar coordinate system has not been considered in the present study. Comparisons of return level sets from inferences in two different coordinate systems were presented in [22] and shown to agree very well, indicating that the results are insensitive to the choice of coordinates.

ACKNOWLEDGMENT

EM was funded by the EPSRC Supergen Offshore Renewable Energy Hub, United Kingdom [grant no: EP/Y016297/1]. CMB acknowledges funding from the EPSRC funded STOR-i centre for doctoral training (EP/L015692/1).

References

[1] S. R. Winterstein, T. C. Ude, C. A. Cornell, P. Bjerager, and S. Haver, "Environmental parameters for extreme response: inverse FORM with omission factors," in *6th International Conference on Structural Safety & Reliability (ICOSSAR)*., 1993.

[2] Q. Derbanne and G. de Hauteclocque, "A new approach for environmental contour and multivariate de-clustering," in *38th International Conference on Ocean, Offshore and Arctic Engineering*, Glasgow, 2019, OMAE2019/95993. DOI: 10.1115/OMAE2019-95993.

[3] E. Mackay and G. de Hauteclocque, "Model-free environmental contours in higher dimensions," *Ocean Engineering*, vol. 273, p. 113 959, 2023. DOI: 10.1016/j.oceaneng.2023.113959.

[4] A. Naess and T. Moan, *Stochastic dynamics of marine structures*. Cambridge University Press, 2013, pp. 1–410.

[5] A. F. Haselsteiner *et al.*, "A benchmarking exercise for environmental contours," *Ocean Engineering*, vol. 236, p. 109 504, 2021. DOI: 10.1016/j.oceaneng.2021.109504.

[6] G. de Hauteclocque, E. Mackay, and E. Vanem, "Quantitative comparison of environmental contour approaches," *Ocean Engineering*, vol. 245, p. 110 374, 2022. DOI: 10.1016/j.oceaneng.2021.110374.

[7] E. Ross *et al.*, "On environmental contours for marine and coastal design," *Ocean Engineering*, vol. 195, p. 106 194, 2020. DOI: 10.1016/j.oceaneng.2019.106194.

[8] S. Haver, "Wave climate off northern Norway," *Applied Ocean Research*, vol. 7, pp. 85–92, 1985. DOI: 10.1016/0141-1187(85)90038-0.

[9] J. Mathisen and E. Bitner-Gregersen, "Joint distributions for significant wave height and wave zero-up-crossing period," *Applied Ocean Research*, vol. 12, no. 2, pp. 93–103, 1990. DOI: 10.1016/S0141-1187(05)80033-1.

[10] R. B. Nelsen, *An introduction to copulas*. Springer, 2006.

[11] H. Joe, *Dependence modeling with copulas*. CRC Press, 2015, pp. 1–457.

[12] F. Silva-González, E. Heredia-Zavoni, and R. Montes-Iturrizaga, "Development of environmental contours using Nataf distribution model," *Ocean Engineering*, vol. 58, pp. 27–34, 2013. DOI: 10.1016/j.oceaneng.2012.08.008.

[13] R. Montes-Iturrizaga and E. Heredia-Zavoni, "Environmental contours using copulas," *Applied Ocean Research*, vol. 52, pp. 125–139, 2015. DOI: 10.1016/j.apor.2015.05.007.

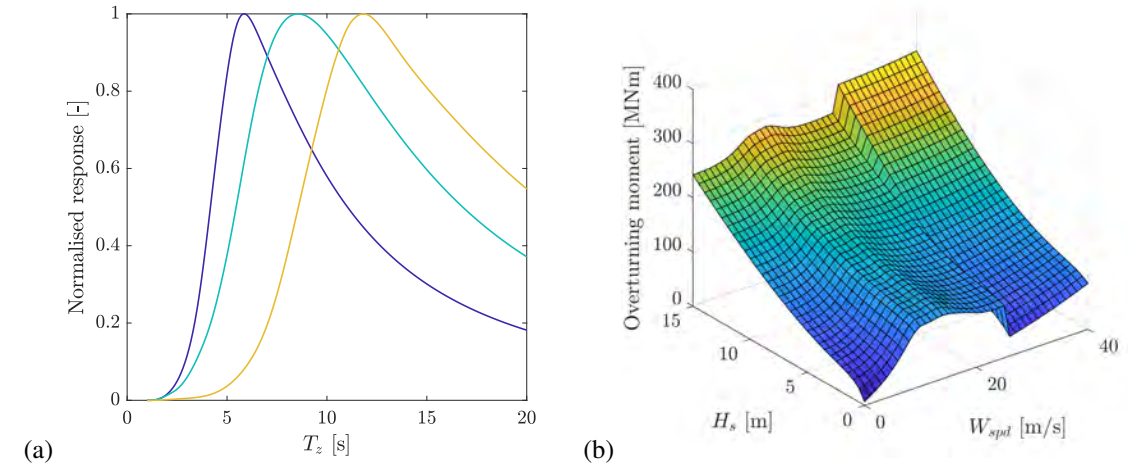

FIGURE 7. EXAMPLE RESPONSE FUNCTIONS. LEFT: NORMALISED RESPONSES FOR FLOATING STRUCTURES (RESPONSES INCREASE LINEARLY WITH H_s). RIGHT: RESPONSE SURFACE FOR OFFSHORE WIND TURBINE.

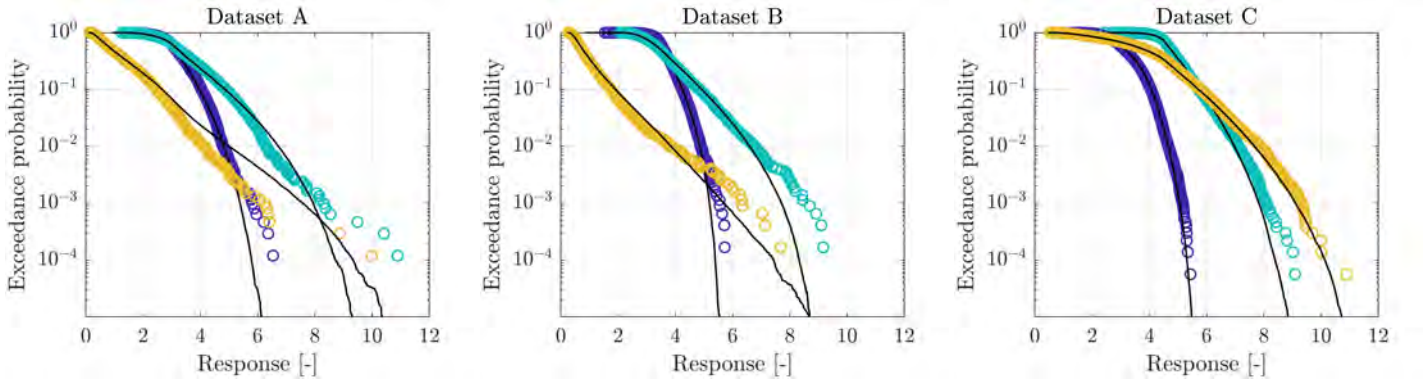

FIGURE 8. COMPARISON OF RESPONSE EXCEEDANCE PROBABILITIES FROM OBSERVATIONS (CIRCLES) AND SPAR MODELS (BLACK LINES) FOR WAVE HEIGHT-PERIOD DATA. COLOUR OF POINTS CORRESPONDS TO RESPONSE FUNCTION SHOWN IN FIGURE 7 (a).

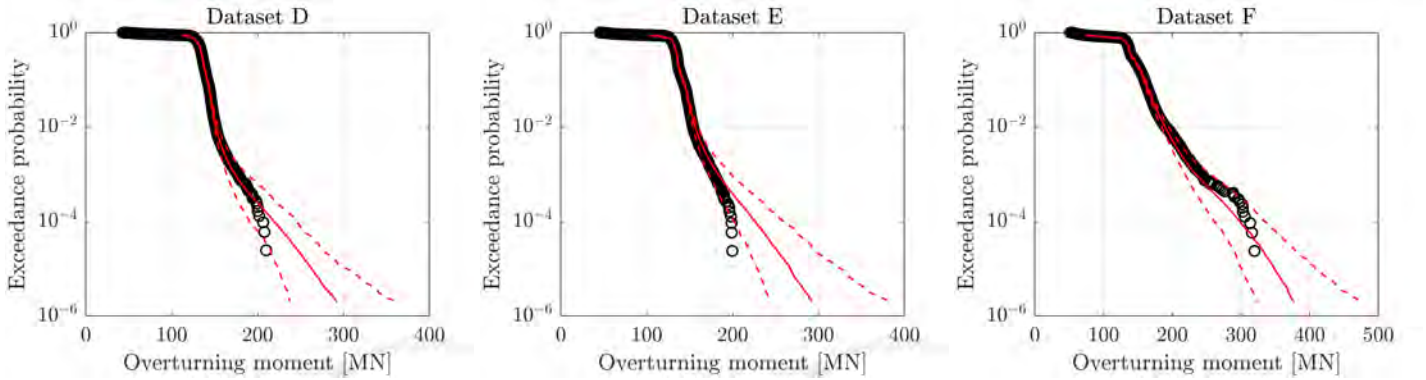

FIGURE 9. COMPARISON OF WIND TURBINE RESPONSE EXCEEDANCE PROBABILITIES FROM OBSERVATIONS (CIRCLES) AND SPAR MODELS (RED LINES). DASHED LINES INDICATE 95% BOUNDS ON MODEL QUANTILES.

[14] R. Montes-Iturrizaga and E. Heredia-Zavoni, "Assessment of uncertainty in environmental contours due to parametric uncertainty in models of the dependence structure between metocean variables," *Applied Ocean Research*, vol. 64, pp. 86–104, 2017. DOI: 10.1016/j.apor.2017.02.006.

[15] P. Jonathan and K. Ewans, "Statistical modelling of extreme ocean environments for marine design: a review," *Ocean Engineering*, vol. 62, pp. 91–109, 2013. DOI: 10.1016/j.oceaneng.2013.01.004.

[16] E. Vanem, T. Zhu, and A. Babanin, "Statistical modelling of the ocean environment–a review of recent developments in theory and applications," *Marine Structures*, vol. 86, p. 103 297, 2022. DOI: 10.1016/j.marstruc.2022.103297.

[17] J. E. Heffernan and J. A. Tawn, "A conditional approach for multivariate extreme values," *J. R. Statist. Soc. B*, vol. 66, pp. 497–546, 2004. DOI: 10.1111/j.1467-9868.2004.02050.x.

[18] B. Gouldby *et al.*, "Multivariate extreme value modelling of sea conditions around the coast of England," *Proc. Institution of Civil Engineers - Maritime Engineering*, vol. 170, pp. 3–20, 2017. DOI: 10.1680/jmaen.2016.16.

[19] E. Ross, S. Sam, D. Randell, G. Feld, and P. Jonathan, "Estimating surge in extreme North Sea storms," *Ocean Engineering*, vol. 154, pp. 430–444, 2018. DOI: 10.1016/j.oceaneng.2018.01.078.

[20] Y. Liu and J. A. Tawn, "Self-consistent estimation of conditional multivariate extreme value distributions," *Journal of Multivariate Analysis*, vol. 127, pp. 19–35, 2014, ISSN: 0047259X. DOI: 10.1016/j.jmva.2014.02.003.

[21] E. Mackay and P. Jonathan, "Modelling multivariate extremes through angular-radial decomposition of the density function," *arXiv*, Oct. 2023. Available: http://arxiv.org/abs/2310.12711.

[22] C. Murphy-Barltrop, E. Mackay, and P. Jonathan, "Inference for multivariate extremes via a semi-parametric angular-radial model," *arXiv preprint (to appear)*, 2023.

[23] S. Coles, *An Introduction to Statistical Modeling of Extreme Values*. Springer, 2001. DOI: 10.1198/tech.2002.s73.

[24] E. Mackay, "Improved models for multivariate metocean extremes," Supergen ORE Hub, Tech. Rep., Jan. 2022. Available: https://supergen-ore.net/uploads/resources/IMEX_final_project_summary.pdf.

[25] S. G. Coles and J. A. Tawn, "Modelling extreme multivariate events," *Journal of the Royal Statistical Society. Series B (Methodological)*, vol. 53, no. 2, pp. 377–392, 1991. DOI: 10.1111/j.2517-6161.1991.tb01830.x.

[26] A. W. Ledford and J. A. Tawn, "Modelling dependence within joint tail regions," *Journal of the Royal Statistical Society . Series B (Methodological)*, vol. 59, no. 2, pp. 475–499, 1997. DOI: 10.1111/1467-9868.00080.

[27] J. L. Wadsworth, J. A. Tawn, A. C. Davison, and D. M. Elton, "Modelling across extremal dependence classes," *Journal of the Royal Statistical Society. Series B: Statistical Methodology*, vol. 79, no. 1, pp. 149–175, 2017. DOI: 10.1111/rssb.12157.

[28] E. Mackay and A. F. Haselsteiner, "Marginal and total exceedance probabilities of environmental contours," *Marine Structures*, vol. 75, p. 102 863, 2021. DOI: 10.1016/j.marstruc.2020.102863.

[29] V. Chavez-Demoulin and A. C. Davison, "Generalized additive modelling of sample extremes," *Journal of the Royal Statistical Society Series C: Applied Statistics*, vol. 54, no. 1, pp. 207–222, 2005. DOI: 10.1111/j.1467-9876.2005.00479.x.

[30] D. Randell, K. Turnbull, K. Ewans, and P. Jonathan, "Bayesian inference for nonstationary marginal extremes," *Environmetrics*, vol. 27, no. 7, pp. 439–450, 2016. DOI: 10.1002/ENV.2403.

[31] B. D. Youngman, "Generalized additive models for exceedances of high thresholds with an application to return level estimation for U.S. wind gusts," *Journal of the American Statistical Association*, vol. 114, no. 528, pp. 1865–1879, 2019. DOI: 10.1080/01621459.2018.1529596.

[32] E. Zanini, E. Eastoe, M. Jones, D. Randell, and P. Jonathan, "Flexible covariate representations for extremes," *Environmetrics*, vol. 31, e2624, 2020. DOI: 10.1002/env.2624.

[33] A. M. Barlow, E. Mackay, E. Eastoe, and P. Jonathan, "A penalised piecewise-linear model for non-stationary extreme value analysis of peaks over threshold," *Ocean Engineering*, vol. 267, p. 113 265, 2023. DOI: 10.1016/j.oceaneng.2022.113265.

[34] S. N. Wood, *Generalized additive models: an introduction with R*. CRC press, 2017.

[35] A. Perperoglou, W. Sauerbrei, M. Abrahamowicz, and M. Schmid, "A review of spline function procedures in r," *BMC medical research methodology*, vol. 19, no. 1, pp. 1–16, 2019. DOI: 10.1186/s12874-019-0666-3.

[36] R. Koenker, *Quantile Regression*. Cambridge University Press, 2005. DOI: 10.1017/CBO9780511754098.

[37] P. J. Northrop and P. Jonathan, "Threshold modelling of spatially dependent non-stationary extremes with application to hurricane-induced wave heights," *Environmetrics*, vol. 22, no. 7, pp. 799–809, 2011. DOI: 10.1002/env.1106.

[38] C. Scarrott and A. MacDonald, "A review of extreme value threshold estimation and uncertainty quantification," *REVSTAT-Statistical journal*, vol. 10, no. 1, pp. 33–60, 2012. DOI: 10.57805/revstat.v10i1.110.

[39] C. Murphy, J. A. Tawn, and Z. Varty, "Automated threshold selection and associated inference uncertainty for univariate extremes," *arXiv*, Oct. 2023. Available: http://arxiv.org/abs/2310.17999.

[40] N. Groll and R. Weisse, "A multi-decadal wind-wave hindcast for the North Sea 1949–2014: coastDat2," *Earth System Science Data*, vol. 9, no. 2, pp. 955–968, 2017. DOI: 10.5194/essd-9-955-2017.

[41] R. Wada, J. Rohmer, Y. Krien, and P. Jonathan, "Statistical estimation of spatial wave extremes for tropical cyclones from small data samples: validation of the STM-E approach using long-term synthetic cyclone data for the Caribbean Sea," *Natural Hazards and Earth System Sciences*, vol. 22, no. 2, pp. 431–444, 2022. DOI: 10.5194/nhess-22-431-2022.

[42] H. R. Kunsch, "The jackknife and the bootstrap for general stationary observations," *The Annals of Statistics*, vol. 17, pp. 1217–1241, 3 1989. DOI: 10.1214/AOS/1176347265.

[43] A. F. Haselsteiner, M. Frieling, E. Mackay, A. Sander, and K.-D. Thoben, "Long-term extreme response of an offshore turbine: how accurate are contour-based estimates?" *Renewable Energy*, vol. 181, pp. 945–965, 2022. DOI: 10.1016/j.renene.2021.09.077.

[44] D. Randell, G. Feld, K. Ewans, and P. Jonathan, "Distributions of return values for ocean wave characteristics in the South China Sea using directional-seasonal extreme value analysis," *Environmetrics*, vol. 26, pp. 442–450, 2015. DOI: 10.1002/env.2350.

[45] H. F. Hansen, D. Randell, A. R. Zeeberg, and P. Jonathan, "Directional–seasonal extreme value analysis of North Sea storm conditions," *Ocean Engineering*, vol. 195, p. 106 665, 2020. DOI: 10.1016/j.oceaneng.2019.106665.

[46] E. Mackay, G. de Hauteclocque, E. Vanem, and P. Jonathan, "The effect of serial correlation in environmental conditions on estimates of extreme events," *Ocean Engineering*, vol. 242, p. 110 092, 2021. DOI: 10.1016/j.oceaneng.2021.110092.

[47] S. Tendijck, P. Jonathan, D. Randell, and J. Tawn, "Temporal evolution of the extreme excursions of multivariate k th order Markov processes with application to oceanographic data," *Environmetrics*, 2023. DOI: 10.1002/env.2834.